Decentralized robust STATCOM control for wind farms to augment dynamic transfer capability

M. J. Hossain[1], H. R. Pota[1], C. Kumble[21, 2]

[1)1] *School of Engineering and Information Technology, UNSW@ADFA, Canberra, ACT-2600, Australia*

[2)2] *Director-Trans. Sec., Hill Michael and Associate, GPO Box 4048 Melbourne Victoria 3001 Australia.*[a)]

(Dated: 6 June 2012)

This paper presents an algorithm to design a decentralized robust controller for STATCOMs (static synchronous compensators) using minimax linear quadratic (LQ) output-feedback control design approach. There is an increase of the available (dynamic) transfer capability (ATC) of power systems with fixed-speed wind generators (FSWGs) due to the designed decentralized controllers. The effects of the integration of various types of wind generators into power systems based on transfer limit has also been analyzed in this paper. The effectiveness of the suggested control strategy is validated by simulations on a benchmark two area power system. The performance of the designed controller is also compared with a conventional PI (proportional-integral)-based STATCOM controller. Simulation results show that both the dynamic voltage stability and the transient stability can be improved by the use of the robust STATCOM control proposed in this paper.

[a)] Electronic mail: m.hossain@adfa.edu.au, h.pota@adfa.edu.au,ckumble@hmac.com.au

I. INTRODUCTION

With growing consumer demands and geographically separated energy sources, large power exchanges over long transmission lines play a vital role in the secure and economic operation of modern power systems. As the power system gets more stressed with increasing loads, the need to transfer power over long transmission lines increases. With political and environmental restrictions on the development of new transmission and generation facilities, it is critical to utilize the total capability of existing transmission lines while also maintaining adequate system reliability.

The obvious and most effective way to increase transmission capability (beyond its thermal rating) is to build a new transmission line. However, this is an expensive solution. If voltage limits and voltage stability are the determining factor for the transfer capability, additional sources of reactive power can be installed at critical location in order to smooth the voltage profile and to increase the reserves against the loss of voltage stability. FACTS devices with suitable controllers allow increased utilization of the existing network, closer to its thermal loading capacity, and avoid the need to construct new transmission lines. Among different FACTS (flexible AC transmission system) devices, STATCOM is being increasingly used for enhancing dynamic voltage stability. STATCOMs with a suitable control strategy have the potential to significantly increase the transient stability margin as well as voltage stability of the system.

Generation of electricity using wind power sources has received considerable attention worldwide in recent years. It has been reported that targets have been set to generate ten to fifteen percent of the world's electricity from wind power by 2020.[1] Wind farms are generally erected in remote areas and it is difficult to control the voltage at these distant places by the use of synchronous generators located at substantial distances. As more and more attention is paid to the increased use of wind farms, a number of complex issues need to be investigated in more detail. Voltage control assessments and reactive power compensation play an increasingly important role during planning and development in determining secure transfer limits for large-scale wind power plants in areas distant from the main power transmission system. It is important to consider the dynamics of wind farms in order to accurately determine the transfer capability.

Transfer capabilities of inter-tie transmission lines establish how much power can be

exchanged between the areas without compromising system viability, voltage security, and dynamic security.[2] In heavily loaded systems voltage stability limit dominates and voltage instability is observed following a large disturbance in a heavily stressed power system with interconnections separated by long distances. Recently more attention is being paid to maintain a healthy voltage profile and design controller for voltage stability. Sufficient attention has not been paid to voltage stability in the determination of the ATC as compared to what has been done for angle stability.

To determine the transfer capability, methods considering thermal and static power-flow analysis have been widely used. In the literature, approaches for the determination of the steady-state limit have been presented taking into account the system limitations linked to steady-state conditions such as maximum loadability, bus voltage and transmission current limits.[3] A technique based on determining voltage stability limits directly associated to voltage collapse conditions (saddle node bifurcation) has been proposed in Ref. 4. An algorithm has been presented in Ref. 5 to evaluate first order effects of network uncertainties such as load forecast error and simultaneous transfers on calculated transfer capability. The dynamics of the power system devices are not considered in these papers.[4,5] Recently the effects of wind power integration on total transfer capability have been investigated using an optimal power-flow technique.[6] This technique does not consider wind farm dynamics and the wind turbine is modeled as a load bus. The behavior of wind turbines during and after disturbances is different from that of conventional generators. During a fault, fixed-speed wind generators draw a large amount of reactive power from the system. This brings out the need to consider the dynamics of wind farms to calculate the dynamic ATC.

Other research directions aim to utilize FACTS devices to enhance transfer capability of certain lines. Optimal placement of FACTS controllers has been studied to maximize the available transfer limit using second order sensitivity analysis.[7] This approach utilizes standard voltage collapse techniques and a variety of static system limits. An optimal power-flow based ATC enhancement model has been formulated to achieve the maximum power transfer for the specified interface with FACTS control, where voltage limits and line thermal limits have been considered.[8] The impact of FACTS devices on ATC and its enhancement has been studied using a genetic algorithm to optimize the best location of an static VAr (volt-ampere reactive) compensator (SVC).[9] In Ref. 10, the effects of FACTS devices on total transfer capability considering thermal, voltage and transient stability limits

of the system have been discussed. Fuzzy control based active and reactive power control of the super-conducting magnetic energy storage (SMES) unit, as well as the control of the transmission line impedance by the static synchronous series capacitor (SSSC) have been studied to increase the maximum loadability of the transmission lines which may be constrained by transient stability limit.[11] Most of the existing works on the enhancement of transfer limit use local FACTS controllers which are designed based on linear models. However, conventional generators and wind generators are highly nonlinear and are coupled with each other.

Modern nonlinear large-scale power systems need more and more sophisticated controllers which require information from the overall network. A decentralized controller, on the other hand is effective and cheap since it does not require information exchange between generator units and is based on local measurements. Because the plant structure and parameter uncertainties always exist, it is also very important to design controllers that are robust to modeling uncertainties. An output- feedback robust decentralized switching control has been proposed recently.[12] In it the operating range is divided into several intervals; one controller is designed for each interval and the controllers are switched depending on the operating point. In practical power systems, it is difficult to implement the switching controllers as unwanted transients may arise due to switching. A decentralized nonlinear controller for large-scale power systems based on the input-output feedback linearization (FBL) methodology has been proposed in Ref. 13. The controllers designed using FBL require the information about the power system topology and the states must be measurable. In practice, it is very difficult to measure all states of the power system. In addition, feedback linearization schemes need exact plant parameters to cancel the inherent system nonlinearities and this makes the stability analysis an involved task.

Wind generator dynamics have considerable effect on the voltage and transient stability of power systems as well as on transfer limits. The literature dealing with the impacts of wind generator dynamics on the ATC is scarce. Section III includes the method, used in this paper, to determine the dynamic ATC and also to analyze the important effects of wind power penetration on the dynamic ATC.

The main contribution in this paper is to present a method for designing a decentralized robust STATCOM controller which enhances dynamic voltage stability as well as transient stability and thereby increases the ATC. For controller design we use the decentralized

minimax linear quadratic output-feedback control design technique. Within the minimax optimal control design framework, robustness is achieved via optimization of the worst-case quadratic performance of the underlying uncertain system.[14] This method achieves an acceptable trade-off between control performance and robustness of the system. The control design in this paper has been tested by simulations under various types of disturbances on a test system. For comparison purposes, the performance of a PI-based STATCOM controller is also evaluated.[15] The comparison shows the superiority of the designed control method over the conventional PI-based STATCOM controller.

The organization of the paper is as follows: Section II provides the mathematical modeling of the power system devices under consideration and discusses the test system. Section III presents an algorithm to determine the ATC; Section IV summarizes the application of the decentralized robust control design technique and presents an algorithm to design the controller; and in Section V, case studies and performance of the controller are outlined. Section VI draws the conclusions.

II. POWER SYSTEM MODEL

In this paper, we consider a benchmark two area power system, which consists of wind generators, conventional generators, STATCOMs, and a mix of constant current, constant impedance, and constant MVA loads. For stability analysis we include the transformer and the transmission line in the reduced admittance matrix. Dynamic models used for the power system devices are presented next.

A. Wind generator

Wind speed and mechanical power extracted from the wind are related as:[16]

$$P_{wt_i} = \frac{\rho_i}{2} A_{wt_i} c_{p_i}(\lambda_i, \theta_i) V_{w_i}^3,$$

for $i = 1, 2, \ldots, n$, where n is total number of generators, P_{wt_i} is the power extracted from the wind in watts, ρ_i is the air density (kg/m^3), c_{p_i} is the performance coefficient or power coefficient, tip speed ratio $\lambda_i = \frac{\omega_{wt_i} R_i}{V_{w_i}}$, R_i is the wind turbine radius (m), ω_{wt_i} is the wind turbine rotational speed (rad/s), V_{w_i} is the wind speed (m/s), θ_i is the pitch angle (degree)

and A_{wt_i} is the area covered by the wind turbine rotor (m^2). A pitch angle controller can be used to control the pitch angle θ_i. The pitch angle controller is active only in high wind speeds and prevents the rotor speed from becoming too high.[16]

A two-mass drive train model of a wind turbine generator system (WTGS) is used in this paper as the drive train model can satisfactorily reproduce the dynamic characteristics of WTGS. The dynamics of the shaft are represented as ($i = 1, 2, \ldots, n$):[16]

$$\dot{\omega}_{wt_i} = \frac{T_{wt_i} - K_{s_i}\gamma_i}{2H_{wt_i}}, \tag{1}$$

$$\dot{\omega}_{m_i} = \frac{K_{s_i}\gamma_i - T_{e_i}}{2H_{wt_i}}, \tag{2}$$

$$\dot{\gamma}_i = 2\pi f(\omega_{wt_i} - \omega_{m_i}), \tag{3}$$

where f represents the nominal grid frequency, T_i is the torque, γ_i is the angular displacement between the two ends of the shaft, ω_i is the speed, H_i is the inertia constant, and K_{s_i} is the shaft stiffness. The subscripts wt_i denote variables related to the ith wind turbine rotor. Similarly, m_i and e_i denote, respectively, mechanical and electrical variables related to the ith generator.

For representation of fixed-speed induction generator models in power system stability studies, the stator flux transients can be neglected in the voltage relations.[17] A simplified transient model of a single cage induction generator (IG) with the stator transients neglected and rotor currents eliminated is described by the following algebraic-differential equations ($i = 1, 2, \ldots, n$):[16,18]

$$V_{ds_i} = R_{s_i} i_{ds_i} - X'_i i_{qs_i} + E'_{dr_i}, \tag{4}$$

$$V_{qs_i} = R_{s_i} i_{ds_i} + X'_i i_{qs_i} + E'_{qr_i}, \tag{5}$$

$$\dot{s}_i = \frac{1}{2H_{m_i}} \left[T_{m_i} - T_{e_i} \right], \tag{6}$$

$$\dot{E}'_{qr_i} = -\frac{1}{T'_{o_i}} \left[E'_{qr_i} - (X_i - X'_i) i_{ds_i} \right] - s_i \omega_s E'_{dr_i}, \tag{7}$$

$$\dot{E}'_{dr_i} = -\frac{1}{T'_{o_i}} \left[E'_{dr_i} + (X_i - X'_i) i_{qs_i} \right] + s_i \omega_s E'_{qr_i}, \tag{8}$$

where $X'_i = X_{s_i} + X_{m_i} X_{r_i}/(X_{m_i} + X_{r_i})$, is the transient reactance, $X_i = X_{s_i} + X_{m_i}$, is the rotor open-circuit reactance, $T'_{o_i} = (L_{r_i} + L_{m_i})/R_{r_i}$, is the transient open-circuit time constant, $P_{s_i} = V_{ds_i} i_{ds_i} + V_{qs_i} i_{qs_i}$, is the real power, $Q_{s_i} = V_{qs_i} i_{ds_i} - V_{ds_i} i_{qs_i}$, is the reactive power, $V_{t_i} = \sqrt{V_{ds_i}^2 + V_{qs_i}^2}$, is the terminal voltage of the IG, s_i is the slip, E'_{dr_i} is the direct-axis transient voltages, E'_{qr_i} is the quadrature-axis transient voltages, V_{ds_i} is the d-axis stator

voltage, V_{qs_i} is the q-axis stator voltage, T_{m_i} is the mechanical torque, T_{e_i} is the electrical torque, X_{s_i} is the stator reactance, X_{r_i} is the rotor reactance, X_{m_i} is the magnetizing reactance, R_{s_i} is the stator resistance, R_{r_i} is the rotor resistance, H_{m_i} is the inertia constant of the IG, $\delta_i = \int_0^t \omega_{r_i} dt$, is the rotor angle, ω_{r_i} is the rotor speed, ω_s is the synchronous speed, i_{ds_i} and i_{qs_i} are d- and q-axis components of the stator current, respectively.

The equations that describe a squirrel cage induction generator (SCIG) are identical to those of the doubly-fed induction generator except that the rotor is short-circuited for SCIG. The converter for variable-speed wind generators used in this paper consist of two voltage source converters connected back-to-back.[16] This enables variable-speed operation of the wind turbines by using a decoupling control scheme which controls the active and reactive components of current separately. A general model for representation of variable-speed wind turbines in power system dynamic simulations has been presented in Ref. 19.

B. Generator

All the generators in this paper have been represented by a sub-transient model. The mechanical input power to the generator is assumed to be constant during the disturbances. The differential equations governing the sub-transient dynamic behavior of the k^{th} generator is given by:[20]

$$\dot{\delta}_k = \omega_k \omega_s - \omega_s, \tag{9}$$

$$\dot{\omega}_k = \frac{1}{2H_k}\left[T_{m_k} - \frac{X''_{d_k} - X_{ls_k}}{X'_{d_k} - X_{ls_k}} E'_{q_k} I_{q_k} - \frac{X'_{d_k} - X''_{d_k}}{X'_{d_k} - X_{ls_k}} \psi_{1d_k} I_{q_k} + \frac{X'_{q_k} - X''_{q_k}}{X'_{q_k} - X_{ls_k}} \psi_{2q_k} I_{d_k} - \frac{X''_{q_k} - X_{ls_k}}{X'_{q_k} - X_{ls_k}} E'_{d_k} I_{d_k} + (X''_{q_k} - X''_{d_k}) I_{q_k} I_{d_k} - D_k \omega_k\right], \tag{10}$$

$$\dot{E}'_{q_k} = \frac{1}{T'_{do_k}}\left[-E'_{q_k} - (X_{d_k} - X'_{d_k})\{-I_{d_k} - \frac{X'_{d_k} - X''_{d_k}}{(X'_{d_k} - X_{ls_k})^2}(\psi_{1d_k} - (X'_{d_k} - X_{ls_k}) I_{d_k} - E'_{q_k})\} + K_{a_k}(V_{ref_k} - V_{t_k} + V_{s_k})\right], \tag{11}$$

$$\dot{E}'_{d_k} = -\frac{1}{T'_{qo_k}}\left[E'_{d_k} + (X_{q_k} - X'_{q_k})\{I_{q_k} - \frac{X'_{q_k} - X''_{q_k}}{(X'_{q_k} - X_{ls_k})^2}(-\psi_{2q_k} + (X'_{q_k} - X_{ls_k}) I_{q_k} - E'_{d_k})\}\right], \tag{12}$$

$$\dot{\psi}_{1d_k} = \frac{1}{T''_{do_k}}\left[-\psi_{1d_k} + E'_{q_k} + (X_{d_k} - X_{ls_k}) I_{d_k}\right], \tag{13}$$

$$\dot{\psi}_{2q_k} = -\frac{1}{T''_{qo_k}} \left[\psi_{2q_k} + E'_{d_k} - (X_{q_k} - X_{ls_k})I_{q_k}\right], \tag{14}$$

for $k = 1, , 2, \ldots, m$, where m is total number of generators, K_{a_k} is AVR (automatic voltage regulator) gain, V_{ti_k} is the terminal voltage, V_{s_k} is the auxiliary input signal to the exciter, δ_k is the power angle of the generator, ω_k is the rotor speed with respect to a synchronous reference, E'_{q_k} is transient emf due to field flux linkage, E'_{d_k} is transient emf due to flux linkage in q-axis damper coil, ψ_{1d_k} is the sub-transient emf due to flux linkage in d-axis damper, ψ_{2q_k} is the sub-transient emf due to flux linkage in q-axis damper, ω_s is the absolute value of the synchronous speed in radians per second, H_k is the inertia constant of the generator, D_k is the damping constant of the generator, T'_{do_k} and T''_{do_k} are direct-axis open-circuit transient and sub-transient time constants, T'_{qo_k} and T''_{qo_k} are q-axis open-circuit transient and sub-transient time constants, I_{d_k} and I_{q_k} d- and q-axis components of stator current, X_{ls_k} is the armature leakage reactance, X_{d_k}, X'_{d_k} and X''_{d_k} are synchronous, transient and sub-transient reactances along d-axis, X_{q_k}, X'_{q_k} and X''_{q_k} are synchronous, transient and sub-transient reactances along q-axis, respectively. The IEEE-ST1A type excitation system is used in this paper.[20]

C. STATCOM

The basic reason of installing a STATCOM in a power system is to provide a controllable AC voltage source. This is done by a voltage source inverter connected to a DC capacitor as shown in Fig. 1. The dynamics of this voltage source is governed by the charging and discharging of a large (nonideal) capacitor. Firing angle α_l controls active power exchange in the converter as well as charge and discharge of DC capacitors and consequently DC-bus voltage v_{dc_l}.

The dynamics for l^{th} STATCOM can be described by the following equation:

$$\dot{v}_{dc_l}(t) = -\frac{P_{s_l}}{C_l v_{dc_l}} - \frac{v_{dc_l}}{R_{C_l} C_l}, \tag{15}$$

for $l = 1, 2, \ldots, p$ where p is total number of STATCOMs, v_{dc_l} is the capacitor voltage, C_l is the DC capacitor, R_{C_l} is the internal resistance of the capacitor, and P_{s_l} is the power supplied by the system to the STATCOM to charge the capacitor. The AC side STATCOM voltage $E_l = k_l v_{dc_l} \angle \alpha_l$, where α_l is the bus angle of the STATCOM in the reduced network, and k_l is a constant associated with the inverter of the STATCOM.

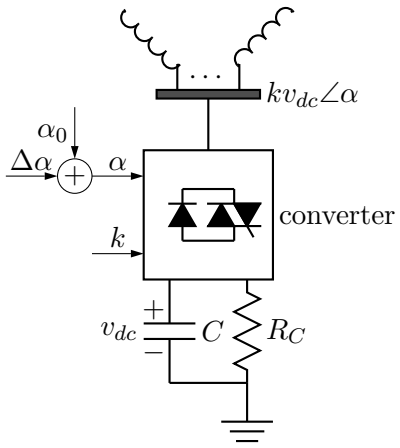

FIG. 1. STATCOM (equivalent circuit)

The terminal voltage of STATCOMs is measured using a transducer with first order dynamic:

$$\dot{v}_{tm_l} = -\frac{v_{tm_l}}{T_{m_l}} + K_{m_l} v_{t_l}, \tag{16}$$

where v_{tm_l} is the sensor output, v_{t_l} is the voltage at the connection point of STATCOM, K_{m_l} is a constant and T_{m_l} is the time constant of the voltage transducer.

D. Test system

The two area test system shown in Fig. 2 consists of 11 buses and 3 generators.[21] The system consists of an area fed by a remote generator G_2 of nominal capacity 2200 MVA through five 500 kV parallel lines. Generator (G_1) models an infinite bus representing a large inertia interconnected system. Area 2 contains a 1600 MVA local synchronous generator G_3 and two aggregate loads, one industrial directly served via the off nominal constant ratio transformer T_4, and one commercial-residential load on bus 11. All the load, P_L = 6655 MW and Q_L = 2021 MVAr, for this test system is in area 2. This load is connected to the transmission network through two transformers (T_5 and T_6) and a 115 kV transmission line between buses 9 and 10. In dynamic simulation, the active components of loads are represented by constant current models and the reactive components by constant impedance models[22]. The base case transfer of power from area 1 to area 2 is 5501 MW. Shunt compensation in area 2 is provided by capacitors C_1 and C_2. The parameters for

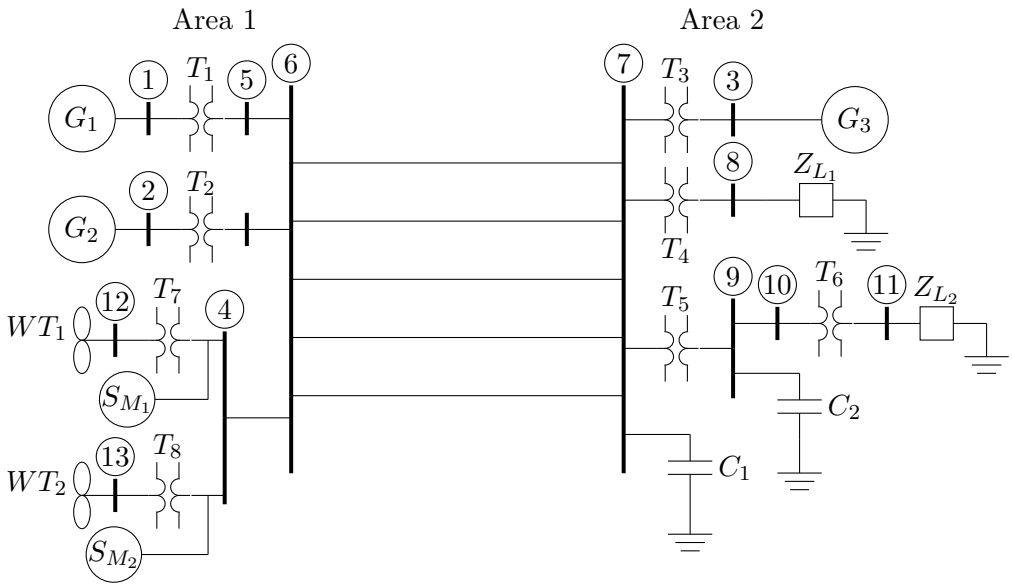

FIG. 2. Test system (G-synchronous generator, WT-wind generator, S_M-STATCOM)

the test system are given in the Appendix. The above described test system is modified by adding two wind farms and a STATCOM at each wind farm as shown in Fig. 2. The effect of wind generation on the ATC is analyzed by varying the mix of conventional and wind generation. The control design is demonstrated for a 5% of the total generation provided by the wind generators in the two wind farms.

The aim of this paper is to design STATCOM controllers to minimize the variation of induction generator slips and thereby improve the ATC. We have designed controllers for STATCOMs, S_{M_1} and S_{M_2}, shown in Fig. 2. For each STATCOM controller, the measured variable is its output voltage and control inputs are the modulation index k_i and firing angle α_i. In this paper k_i has been fixed and α_i is used as the control variable. The increase in dynamic ATC, between the two areas separated by transmission lines between bus 6 and bus 7, due to the designed controller is demonstrated in this paper.

The ATC is determined using the full nonlinear model of the test system. Controllers are designed using a linearized model of the system. As mentioned previously, owing to the nature of the control problem, decentralized controllers are designed for each STATCOM and an excitation controller is implemented for the generator G_3.

III. ALGORITHM FOR DYNAMIC ATC ASSESSMENT

A number of methods for computing the ATC have been reported in the literature. Continuation power-flow methods repeat full-scale AC load-flow solution for each increment of the load above the base case value at the sink bus until a line in the system is overloaded.[5] Although accurate, these methods are not real-time compatible for large systems. As an alternative there exist DC load-flow based methods which are a bit faster than their AC counterparts but they model only real power-flow in the lines and assume the network to be lossless.[23]

Methods based on power transfer or outage distribution factors can cater only to the scenarios that are too close to the base case from which these factors are derived.[24] The reported artificial neural network method requires a large input vector so that it has to oversimplify determination of ATC by limiting it to a special case of power transfer to a single area from all of the remaining areas.[25] This method is unable to track down the bus-to-bus transactions, which is the true spirit of deregulation.

In this paper, the following procedure is used to analyze the ATC and verify the performance of the designed controller:[26]

(i) Select the base case and solve the power-flow;

(ii) Make a step increase in generation and load, solve the power-flow problem according to the modified system condition;

(iii) Conduct a stability analysis to check the security limit for large disturbances with the complete nonlinear model;

(iv) If the security limit is acceptable, go to (ii), otherwise go to (v);

(v) The highest feasible increment denotes how much power can additionally be transmitted for the given base scenario.

IV. DECENTRALIZED ROBUST CONTROL

This section presents all the equations required to design decentralized STATCOM controllers. The control design is based on recent works on the decentralized minimax output-

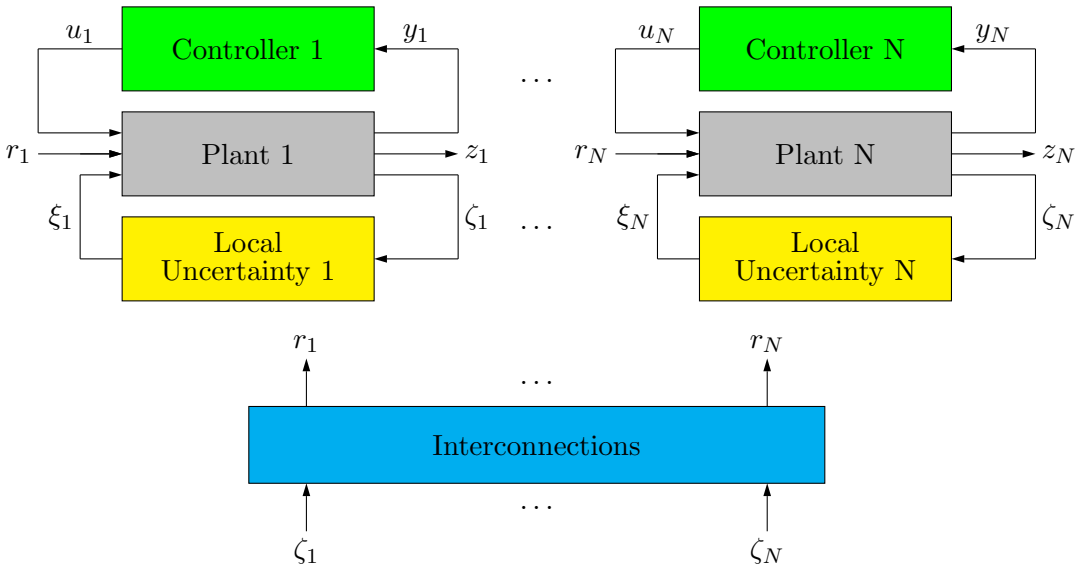

FIG. 3. Block diagram of the uncertain system.

feedback control.[12,27] The power system model used in this paper is described by the following form where a large scale system S comprising N subsystems S_i, $i = 1, 2, \ldots N$,

$$S_i : \dot{x}_i(t) = A_i x_i(t) + B_i u_i(t) + E_i \xi_i(t) + L_i r_i(t), \tag{17}$$

$$z_i(t) = C_i x_i(t) + D_i \xi_i(t), \tag{18}$$

$$\zeta_i = H_i x_i(t) + G_i u_i(t), \tag{19}$$

$$y_i = C_{y_i} x_i(t) + D_{y_i} \xi_i(t), \tag{20}$$

where $x_i \in R^{ni}$ is the state vector, $u_i \in R^{mi}$ is the control input, $\xi_i \in R^{pi}$ is the perturbation, $\zeta_i \in R^{hi}$ is the uncertainty output, $z_i \in R^{qi}$ is the controlled output, $y_i \in R^{gi}$ is the measured output, and the input r_i describes the effect of the other subsystems $S_1, \ldots, S_{i-1}, S_{i+1}, \ldots, S_N$ on subsystem S_i. The structure of the system S is shown in Fig. 3. The system model (17)-(20) reflects the nature of a generic interconnected uncertain system in which each subsystem is affected by uncertainties that have two sources. Local uncertainties in the large scale system arise from the presence of uncertain dynamics in each subsystem. Such dynamics are driven only by the uncertainty output ζ_i of the subsystem S_i. A second source of uncertainties arises from interactions between the subsystems of the large scale system. Indeed, the partition of a complex uncertain system into a collection of subsystems S_i results in the uncertainty in the original system being distributed amongst the subsystems. This provides the motivation for treating the interconnections as uncertain perturbations.

The matrices D_i, G_i and D_{yi} are chosen in such a way that the following assumptions hold. We assume that the power system under consideration satisfies the following assumptions:[12]

- **Assumptions 1**: For all $i = 1, \ldots, N$, $D_i^T D_i + G_i^T G_i > 0$, $D_{y_i} D_{y_i}^T > 0$.
- **Assumptions 2**: The pair $(A_i, C_i^T C_i)$, $i = 1, \ldots, N$, is observable.
- **Assumptions 3**: The pair (A_i, B_i), $i = 1, \ldots, N$, is stabilizable.

We also define $\xi_i = \triangle_i \zeta_i$ and $r_i = \sum_{j \neq i} \tilde{\triangle}_{ij} \zeta_j$, where $\triangle_i$ and $\tilde{\triangle}_{ij}$ are uncertain gain matrices. The uncertainty and interconnections satisfy the following conditions:

$$\|\xi_i(t)\|^2 \leq \|\zeta_i(t)\|^2 \text{ and } \|r_i(t)\|^2 \leq \sum_{j \neq i} \|\zeta_j(t)\|^2. \tag{21}$$

The minimax output-feedback controller designed in this paper minimizes the following cost subject to the above (21) bounds on the local uncertainty and interconnections:

$$\int_0^\infty \sum_{i=1}^N \|z_i(t)\|^2 dt. \tag{22}$$

In this paper we consider norm bounded constraints, as in (21), instead of the more general IQCs (integral quadratic constraints). This means that the designed controllers are suboptimal for norm bounded constraints. As described in Ref. 12, the control algorithm finds the infimum of the right-hand-side of the following function over the set $\mathcal{T}$:

$$\inf_{u_i,\ i=1,\ldots,N} \sup_{\Xi,\Pi} \int_0^\infty \sum_{i=1}^N \|z_i(t)\|^2 dt \leq \inf_{\mathcal{T}} \sum_{i=1}^N x_{i0}^T \left[X_i + \tau_i M_i + \theta_i \bar{M}_i \right] x_{i0}, \tag{23}$$

where $[x_{10}, \ldots, x_{N0}]^T$ is the initial condition vector, Ξ is a set of all admissible uncertainties, Π is a set of admissible interconnection inputs, a set of vectors $\mathcal{T} = \{\{\tau_i\ \theta_i\}_{i=1}^N \in R^{2N}\}$, $M_i > 0$ and $\bar{M}_i > 0$ are two positive definite symmetric matrices which satisfy the following conditions:

$$E \int_0^{t_l} \left(\|\zeta_i(t)\|^2 - \|\xi_i(t)\|^2 \right) dt > -x_{i0}' M_i x_{i0}, \tag{24}$$

$$E \int_0^{t_l} \left(\sum_{n=1, n \neq i}^N \|\zeta_n(t)\|^2 - \|r_i(t)\|^2 \right) dt > -x_{i0}' \bar{M}_i x_{i0}, \tag{25}$$

where E is the expectation operator, $\{t_l\}_{l=1}^\infty, t_l \to +\infty$ is a sequence, $M_i = M_i' > 0$, $\bar{M}_i = \bar{M}'_i > 0$. Equations (24) and (25) allow to account for effects of non-zero initial

conditions of uncertain dynamics in the local uncertainty channels and interconnections. The term on the right hand sides of IQCs (24) and (25) correspond to bound on these uncertainties. Those bounds can be written as quadratic forms $x'_{i0}M_i x_{i0}$, and $x'_{i0}\bar{M}_i x_{i0}$.[14]

The matrices X_i and Y_i are the solutions of the following pair of parameter dependent coupled generalized algebraic Riccati Eqs.:[27]

$$A_i^T Y_i + Y_i A_i + Y_i \bar{B}_{2_i} \bar{B}_{2_i}^T Y_i - \left[C_{y_i}^T W_i^{-1} C_{y_i} - \bar{C}_i^T \bar{C}_i\right] = 0, \tag{26}$$

$$A_i^T X_i + X_i A_i + \bar{C^T}_i \bar{C}_i - X_i \left[B_i R_i^{-1} B_i^T - \bar{B}_{2_i} \bar{B}_{2_i}^T\right] X_i = 0, \tag{27}$$

where $R_i = \bar{D}_i^T \bar{D}_i$, $W_i = \bar{D}_{y_i} \bar{D}_{y_i}^T$, $\bar{\theta}_i = \sum_{n=1, n\neq i}^{N} \theta_n$,

$$\bar{C}_i = \begin{bmatrix} C_i \\ (\tau_i + \bar{\theta}_i)^{1/2} H_i \end{bmatrix}, \quad \bar{D}_i = \begin{bmatrix} D_i \\ (\tau_i + \bar{\theta}_i)^{1/2} G_i \end{bmatrix},$$

$$\bar{B}_{2_i} = \left[\tau_i^{-1/2} E_i \;\; \theta_i^{-1/2} L_i\right], \quad \bar{D}_{y_i} = \left[\tau_i^{-1/2} D_{y_i} \;\; 0\right].$$

Then the controller is designed with the Eqs.:[12]

$$\begin{aligned} \dot{x}_{c_i} = &\{A_i - \left[B_i R^{-1} B_i^T - \bar{B}_{2_i} \bar{B}_{2_i}^T\right] X_i\} x_{c_i} \\ &+ \left[Y_i - X_i\right]^{-1} C_{y_i}^T W_i^{-1} \left[y_i(t) - C_{y_i} x_{c_i}(t)\right], \end{aligned} \tag{28}$$

$$u_i = -R_i^{-1} B_i^T X_i x_{c_i}. \tag{29}$$

The solutions are required to satisfy the following conditions: $\tau_i > 0$, $\theta_i > 0$, $X_i \geq 0$, $Y_i \geq 0$ and $Y_i > X_i$.

A. Controller design for the test system

The problem considered here is of designing a robust LQ output-feedback decentralized STATCOM control, which works in the presence of interconnection effects. To demonstrate the control design process, controllers are designed for two 12.5 MVAr STATCOMs connected to the two wind farms, and an excitation controller for generator G_3. The STATCOMs S_{M_1}, S_{M_2}, and the wind generators WT_1, WT_2 are shown in Fig. 2. The two wind farms are equipped with fixed-speed wind generators and supply 5% of the total load. We represent each wind farm by an aggregated wind generator model.[28]

Modal analysis is performed on the interconnected system to get an idea of the dominant modes which need to be controlled.[21] The dominant mode for the test system is

TABLE I. Participation factors

States	$\triangle s_1$	$\triangle E'_{qr_1}$	$\triangle s_2$	$\triangle E'_{qr_2}$	$\triangle \omega_3$	$\triangle \delta_3$
Participation Factor	0.96	1.0	0.94	0.97	0.89	0.32

$-0.0985 \pm \jmath 3.463$ with damping ratio 0.028. The normalized significantly contributing participation vector for the dominant mode is shown in Table I. From the participation vector it is clear that both of the wind farms contribute significantly to the dominant mode and hence controllers should be designed for both the wind generators. This brings out the need to design decentralized controllers. The test system considered in this paper is divided into three subsystems: (i) Wind Farm 1 and STATCOM 1 (ii) Wind Farm 2 and STATCOM 2 (iii) G_1, G_2, and G_3. The STATCOM controllers are designed for subsystems 1 and 2, and an excitation controller is designed for subsystem 3 and it is implemented on generator G_3. All the generators and exciters are represented by an aggregated equivalent seventh-order model. [29]

The first step to design the controller for STATCOMs is to determine the matrices and define the variables in problem formulation (17)-(20).

To obtain the subsystem matrices in (17)-(20), the complete system is first linearized about the desired equilibrium point. For each subsystem the state variables are divided into two parts. One part consists of the states of the devices in the subsystem, called x_i and the other part consists of the rest of the states, called r_i. The matrices A_i and L_i are appropriately chosen from the complete linearized model equations.

1. Subsystems 1 and 2

The uncertainty output ζ_i and the perturbation input ξ_i are chosen such that

$$\zeta_i = [\Delta s_i, \Delta E_{dr_i}, \Delta E_{qr_i}, \Delta v_{dc_i}]^T, \text{ and } \xi_i = \zeta_i.$$

Owing to this choice of uncertainty output and perturbation input the inequalities in (21) are satisfied. The state vector for wind farm subsystems is ($i = 1, 2$):

$$x_i = [\Delta\omega_{wt_i}, \Delta\omega_{m_i}, \Delta\gamma_i, \Delta s_i, \Delta E_{dr_i}, \Delta E_{qr_i}, \Delta v_{dc_i}, \Delta v_{tm_i}]^T.$$

The uncertainty term, represented by $E_i\xi_i$, is obtained by increasing the load by ten percent, finding the new equilibrium point, linearizing the system about that point, and taking the difference between the subsystem A-matrices for the nominal load and the increased load.[30] This difference in A-matrices is E_i.

For the subsystems with wind generators ($i = 1, 2$):

$$C_i = \begin{bmatrix} 0 & 0 & 0 & 1 & 0 & 0 & 0 & 0 \end{bmatrix}, \; C_{yi} = \begin{bmatrix} 0 & 0 & 0 & 0 & 0 & 0 & 0 & 1 \end{bmatrix}, \; H_i = \begin{bmatrix} 0 & 0 & 0 & 1 & 0 & 0 & 0 & 0 \\ 0 & 0 & 0 & 0 & 1 & 0 & 0 & 0 \\ 0 & 0 & 0 & 0 & 0 & 1 & 0 & 0 \\ 0 & 0 & 0 & 0 & 0 & 0 & 1 & 0 \end{bmatrix}. \quad (30)$$

The above choice of matrices means that the controlled output is the variation in induction generator slip and the measured output is the change in STATCOM terminal voltage. The control input is the firing angle α_i of the STATCOMs.

Matrices D_i, G_i, and D_{yi} for the subsystems with wind generators are chosen as follows:

$$D_i = 10^{-4} \begin{bmatrix} 1 & 1 \end{bmatrix}, \; G_i = 10^{-6} \begin{bmatrix} 1 & 1 \\ 1 & 1 \\ 1 & 1 \\ 1 & 1 \end{bmatrix}, \; D_{yi} = 10^{-4} \begin{bmatrix} 0 & 0 & 0 & 1 & 1 & 1 & 1 & 0 \end{bmatrix}.$$

$$x_{i0} = \begin{bmatrix} 0.1 & \dots & 0.1 \end{bmatrix}^T,. \quad (31)$$

2. *Subsystem 3*

The uncertainty output ζ_3 and the perturbation input ξ_3 are chosen such that

$$\zeta_3 = \left[\Delta E'_q, \Delta E'_d, \Delta\psi_{1d}, \Delta\psi_{2q}\right]^T, \text{ and } \xi_3 = \zeta_3.$$

Matrices for the subsystem 3 with all the generators are:

$$C_3 = \begin{bmatrix} 1 & 0 & 0 & 0 & 0 & 0 & 0 \end{bmatrix}, \; C_{y3} = \begin{bmatrix} 0 & 1 & 0 & 0 & 0 & 0 & 0 \end{bmatrix}, \; H_3 = \begin{bmatrix} 0 & 0 & 1 & 0 & 0 & 0 & 0 \\ 0 & 0 & 0 & 1 & 0 & 0 & 0 \\ 0 & 0 & 0 & 0 & 1 & 0 & 0 \\ 0 & 0 & 0 & 0 & 0 & 1 & 0 \end{bmatrix}. \quad (32)$$

This choice means that the controlled variable is the generator angle deviation and the measured variable is the speed deviation from the synchronous speed. The other matrices in the subsystem model representation are:

$$D_3 = 10^{-6},\ G_3 = 10^{-6}\begin{bmatrix}0 & 0 & 0 & 1\end{bmatrix}^T,\ D_{y3} = 10^{-4}\begin{bmatrix}0 & 0 & 1 & 1 & 1 & 1 & 0\end{bmatrix}, \tag{33}$$
$$x_{30} = [0.1, \ldots, 0.1]^T.$$

The matrices $M_i, \bar{M}_i$ can be chosen to be arbitrary positive definite matrices; we select them as identity matrices.

The algorithm to design the proposed controller can be summarized as follows:

- **Step 1**: For a given equilibrium point, obtain matrices in (17)–(20) according to the procedure outlined in Section IV.
- **Step 2**: Solve the optimization problem (23). This is done by using a line search technique for positive values of τ_i and θ_i. Matlab function *fmincon* can be used to do the line search with a proper initialization. In the design presented in this paper the line search was initialized with $\tau_i = 0.0015$ and $\theta_i = 0.000015$. For this case the function *fmincon* converges without any perceptible delay. To be certain that the solution is not numerically ill-conditioned, it is ensured that the solution of the Eqs. (26)-(27) gives positive definite X_i and Y_i for the values of τ_i and $\theta_i, i = 1, \ldots, N$ at which the infimum is achieved in (23).
- **Step 3**: Substitute the optimizing values of τ_i and θ_i into the Riccati Eqs. (26), (27) and obtain X_i and Y_i.
- **Step 4**: The designed controllers are given by Eqs. (28)–(29).

For the test system considered in this paper, the optimum value of the objective function is obtained for $\tau_1 = 0.0645$, $\tau_2 = 0.0468$, $\tau_3 = 0.0167$, $\theta_1 = 0.0005$, $\theta_2 = 0.0045$, and $\theta_3 = 0.0001$. The optimal minimax value of the performance cost for the test system is 0.2156 with 5% wind generator integration and 2×12.5 MVA STATCOMs.

V. CASE STUDIES AND CONTROLLER PERFORMANCE EVALUATION

To evaluate the controller performance the ATC is calculated by increasing load in area 2 and the generation in area 1. For security assessment, we apply a three-phase fault on middle

of one of the transmission lines between bus 6 and bus 7. The fault is cleared after five cycles by opening the line and the line is restored after further five cycles. In load-flow analysis, the acceptable voltage range considered in this paper is 0.9–1.1 pu. The dynamic ATC with conventional generator, evaluated using the method in Section III for the three-phase fault contingency is 690 MW.

The following analysis is divided into three parts: (a) Effect of different levels of wind generator integration on the ATC, (b) Determination of compensations to restore and enhance the ATC with FSIGs, and (c) Robust STATCOM controller performance evaluation in increasing the ATC.

A. Effect of wind generator integration on ATC

To show the effect of the wind turbines on transfer capability, a portion of the generation provided by G_1 and G_2 is provided by the wind farms. In the first case, five percent of the conventional power in area 1 is replaced by fixed-speed wind turbines. In this case the ATC is reduced to 569 MW as compared to 690 MW with only conventional generation.

In the second case, we use variable-speed wind turbines instead of fixed-speed induction generators. A variable-speed wind turbine with a doubly-fed induction generator uses constant terminal voltage or unity power factor operation depending on the operating conditions. For the same penetration level and variable-speed wind turbines (VSWT) with terminal voltage control, the ATC is 689 MW. The ATC is 720 MW with the VSWT operated in the power factor control mode (0.95 leading).

It is clear that with variable-speed wind turbine in voltage control mode the ATC changes only slightly, whereas the fixed-speed wind turbine reduces the ATC by 17.53%. The variable-speed wind turbine operating at leading power factor 0.95 increases the ATC by 4.34%.

The variation of the ATC with the varying amount of penetration of FSWGs is shown in Fig. 4. The numerical values are given in Table II. It can be seen from Fig. 4 that initially the ATC decreases gradually and after 7.5% penetration there is a sharp decrease in the ATC. This sudden drop underscores the importance of a thorough analysis before replacing conventional generation with wind power.

TABLE II. Effect of FSIG on the ATC and compensations to restore it

FSIG integration in %	0	2.5	5	7.5	10
ATC in MW	690	643.5	607	545	90
STATCOM in MVA	0	12.5	25	44	81
Capacitor in MVAr	0	60	100	160	300

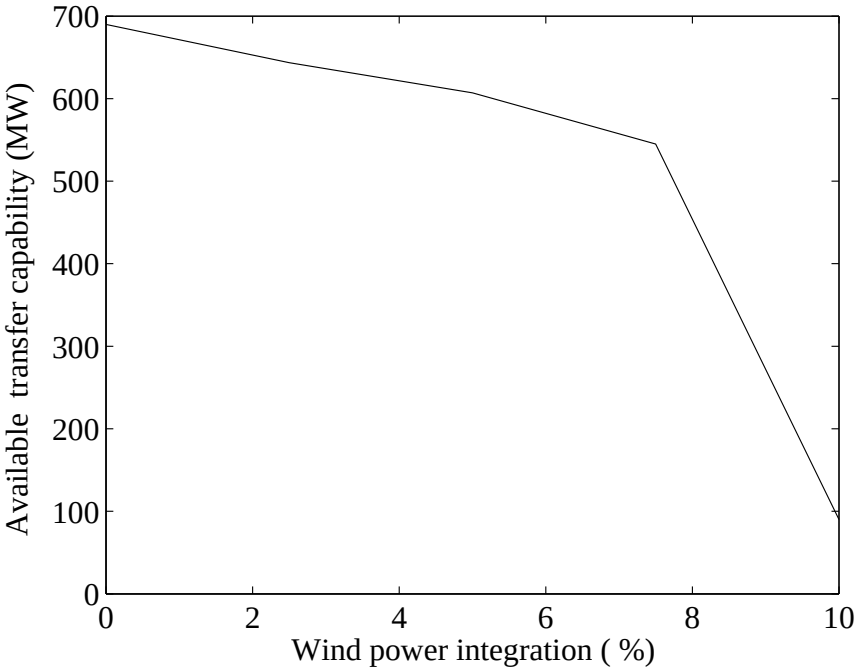

FIG. 4. Change in ATC due to FSIG integration.

B. Compensations to restore the ATC with FSIG

Wind generators are generally connected with power capacitors to improve the power factor. The amount of compensations (both static and dynamic) to restore the deficiency in ATC due to fixed-speed wind generator integration is shown in Fig. 5. For a five percent wind power integration, 2×50 MVAr capacitors are required to restore the ATC to 690 MW. Two 12.5 MVAr capacity STATCOMs with the designed control can replace the 2×50 MVAr static capacitors with superior dynamic response. The cost of capacitors is \$10 to \$20 per kVAr, and STATCOMs cost \$55 to \$70 per kVAr for systems with a capacity of 100 MVAr or more.[31] The use of STATCOMs does not reduce the cost but they enhance the

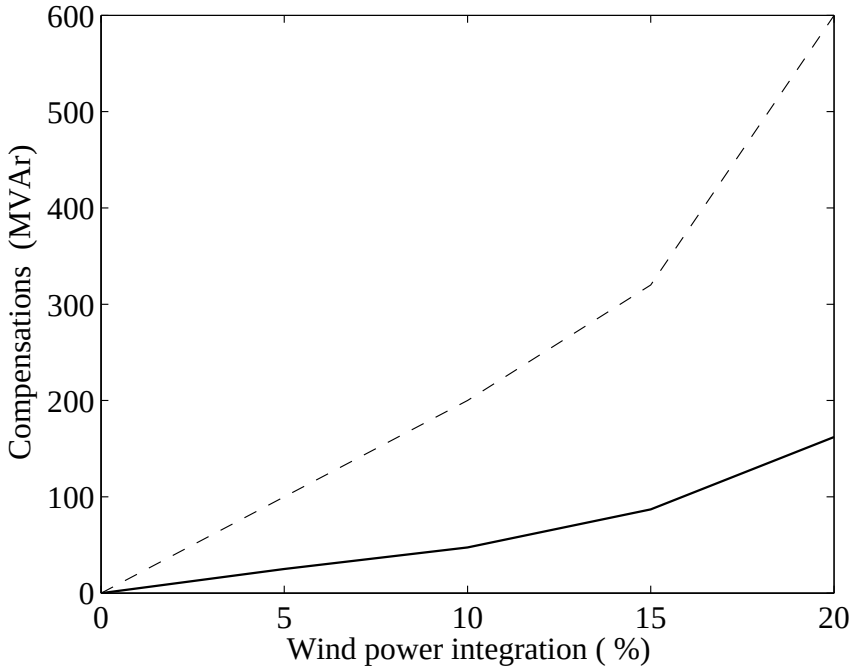

FIG. 5. Compensations to restore the ATC. (The solid line represents STATCOM rating, and dash line capacitor bank.)

dynamic performance significantly. The reactive power delivered by the shunt capacitor is proportional to the square of the terminal voltage, which means that during low-voltage conditions VAr support drops, thus compounding the problem. The STATCOM provides extra reactive power support dynamically with a continuous change of output for voltage recovery when the voltage becomes low.

C. Controller performance evaluation

For a 5% wind energy penetration and 2×12.5 MVA STATCOM controllers designed in this paper, the dominant mode for the closed-loop system is $-0.424 \pm \jmath 0.47831$ with the damping ratio 0.66291. From this it is clear that the closed-loop system is well-damped. In contrast the critical mode for open-loop system with 2×50 MVAr capacitors is $-0.1578 \pm \jmath 2.6$ and the damping ratio is only 0.061.

The performance of the designed robust decentralized STATCOM controller is tested by simulating response to two contingencies on the test system. The contingencies are: (a) the outage of one transmission line and (b) three-phase short circuit at the middle of one of the

transmission lines between bus 6 and bus 7.

1. Outage of one transmission line

Transmission line outage increases the line impedance and weakens the interconnection. Due to the increase in the line reactance, extra reactive power is needed in order to maintain the voltage at the load bus. The STATCOM voltage controller responds to this condition by increasing the reactive power output and this has a beneficial effect on the voltage stability.

Simulation is performed with the line opened at $t = 1$s and subsequently reclosed after 0.15s. Fig. 6 shows the load voltage at bus 11 due to outage of one of the transmission lines between bus 6 and bus 7, with (i) 2×50 MVAr static capacitor banks, (ii) the designed controllers for 2×12.5 MVA STATCOMs. The steady-state value for load voltage at bus 11 for conditions (i) and (ii) are 1.066 pu and 1.00 pu respectively. From Fig. 6, it can be seen that STATCOM controllers provides better dynamic performance as compared to the 2×50 MVAr capacitor banks in terms of both damping, overshoot and settling time. This behavior is explained by the low damping (0.061) of the open-loop system with fixed capacitor compensation. For the total of 90 MVAr and below of fixed capacitor compensation, the system is not able to recover to the pre-fault voltage.

2. Three-phase short circuit

One of the most severe disturbances leading to voltage collapse is a three-phase fault on one of the key transmission circuits. In this simulation a symmetrical three-phase fault is applied at the middle of one of the transmission lines between bus 6 and bus 7. The fault is cleared after five cycles. Fig. 7 depicts variation of the PCC (point of common coupling) voltage at bus 4. The power transferred through the line 4–6 is shown in Figs. 8 and 9. From Figs. 8 and 9, it can be concluded that more power can be transmitted through the transmission line with the designed STATCOM controllers during transient. The reactive power drawn by wind generators and supplied by STATCOM is shown in Fig. 10. It can be seen that the total reactive power output of STATCOMs is in phase of the reactive power consumed by the wind generators.

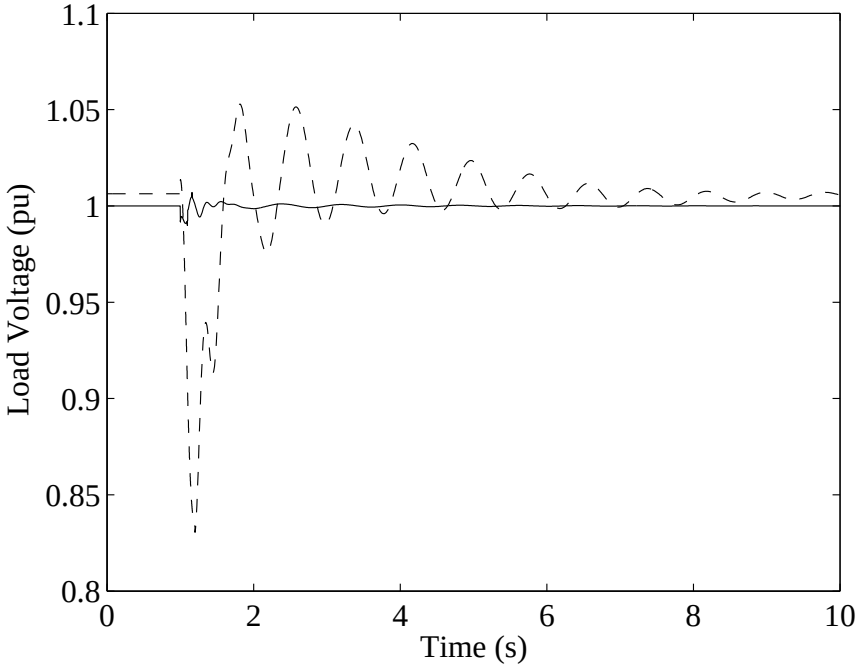

FIG. 6. Load voltage for outage of one of the lines 6-7. (The solid line represents designed STATCOM control response, and dash line capacitor bank.)

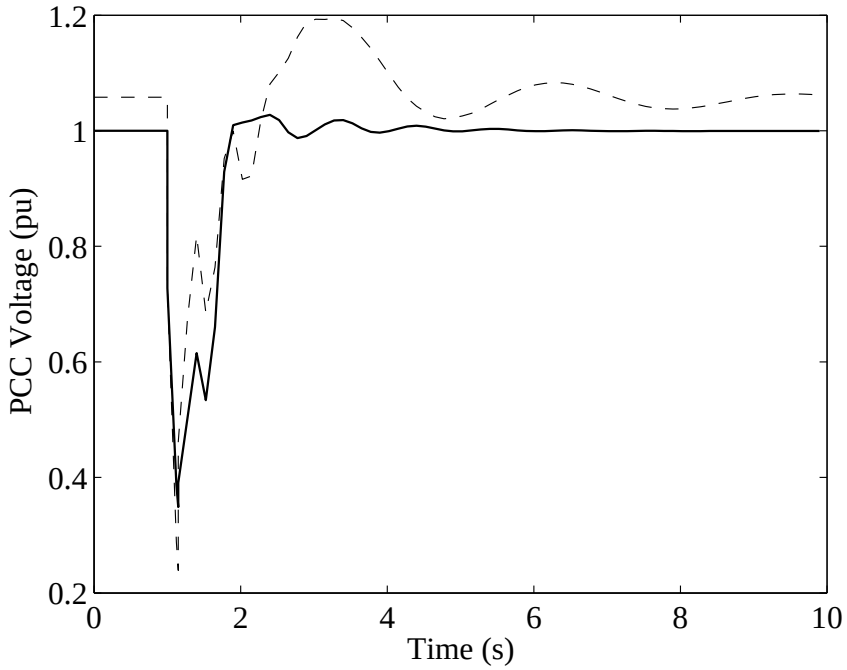

FIG. 7. PCC voltage for a three phase fault on middle of one of the lines 6–7. (The solid line represents designed STATCOM control response, and dash line capacitor bank.)

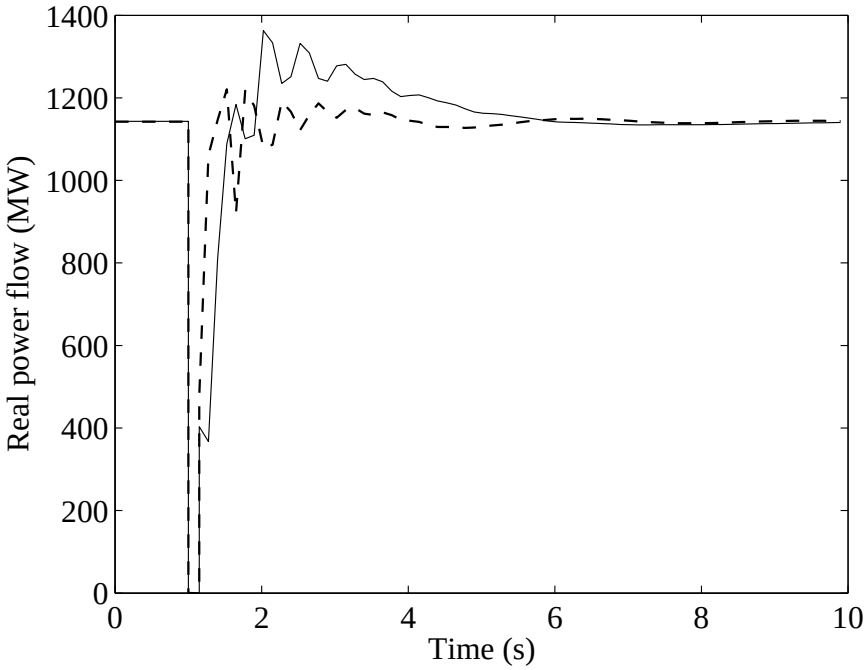

FIG. 8. Real power flow through the line 4–6 for a three phase fault on middle of one of the lines 6–7. (The solid line represents designed STATCOM control response, and dash line capacitor bank.)

3. Comparison with PI-based STATCOM

To evaluate the designed controller performance the dynamic ATC is calculated with five percent FSIGs using PI-based STATCOM control and the proposed robust STATCOM controller. The maximum ATC with PI-based STATCOM is 687 MW, whereas with the proposed robust STATCOM control is 698 MW, i.e., the ATC is increased by 1.6% using this robust control algorithm.

To test the dynamic performance, a simulation is performed with the increased ATC (698 MW) by applying the same three-phase fault as in the previous simulation. Figs. 11 and 12 show the load voltage at bus 11 and speed of a wind generator (WF_1) with the proposed STATCOM control and with a PI-based STATCOM controller. With the PI control, the speed continues to increase due to the imbalance between the mechanical power extracted from the wind and electrical power delivered to the grid even after the fault is cleared. When a disturbance or fault occurs, the voltage at the terminals of the wind turbine drops significantly, causing the electromagnetic torque and electric power output of the generator

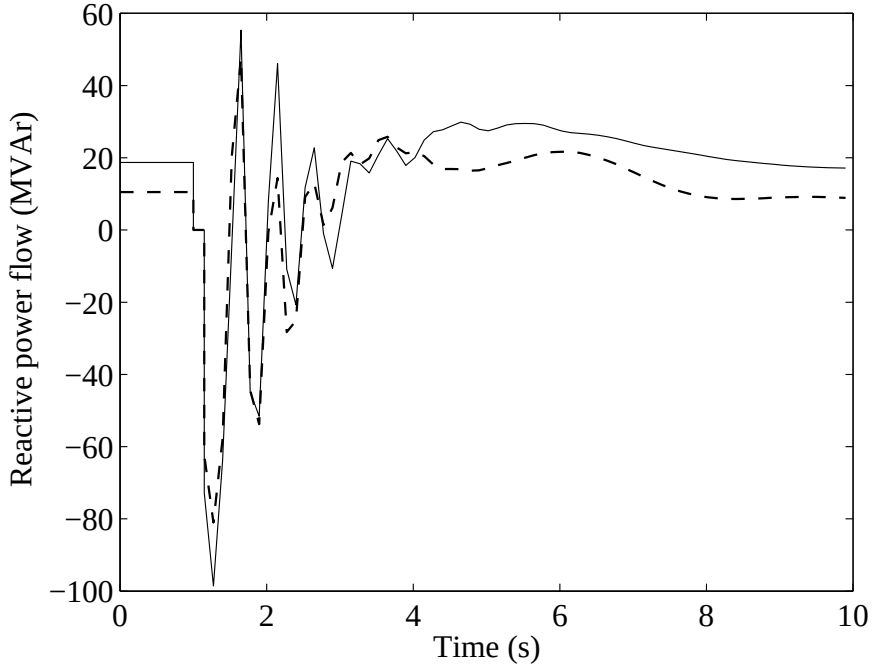

FIG. 9. Reactive power flow through the line 4–6 for a three phase fault on middle of one of the lines 6–7. (The solid line represents designed STATCOM control response, and dash line capacitor bank.)

to be greatly reduced. However, given that the mechanical input torque is almost constant when typical non-permanent faults occur in a wind farm, this leads to an acceleration of the machine rotor. Furthermore, the voltage gradually decreases and the wind generators have to be disconnected from the grid to protect them and avoid voltage collapse.

The reference input for the each PI-based STATCOM controller in this paper has reactive power (Q_{ref}=12.5 MVAr). For this reference reactive power, the load-flow converges for two different values of the load voltage at bus 11, 1.0 pu and 0.6 pu. In this simulation the post fault voltage with PI-based STATCOM settles to the lower 0.6 pu voltage equilibrium point. The designed controller provides a satisfactory dynamic response for this contingency. From this we conclude that the proposed controller performs better than the conventional PI-based controller both in terms of transfer capability and dynamic performance of the system.

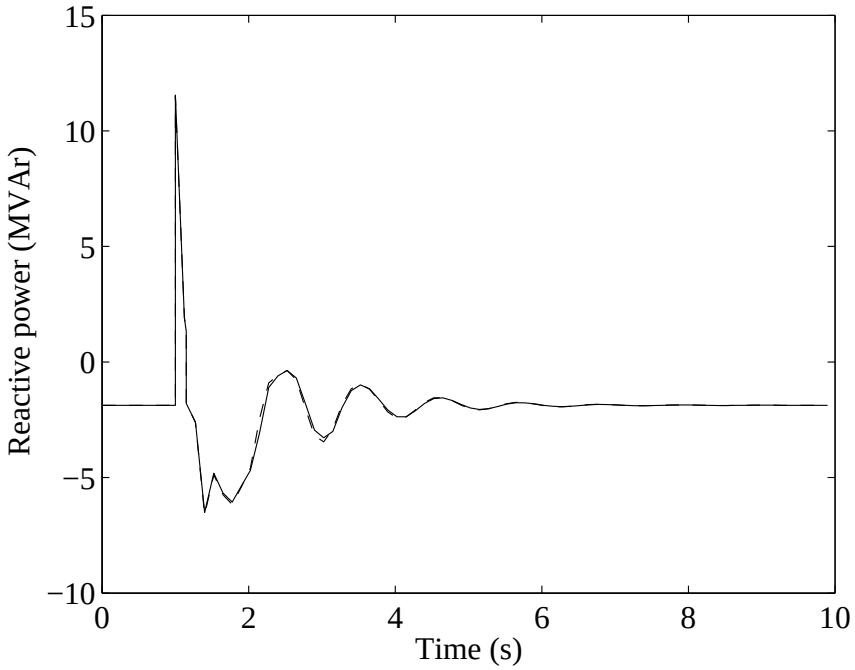

FIG. 10. Reactive power for a three phase fault on middle of one of the lines 6–7. (The solid line represents reactive power output by the designed STATCOM (S_{M_1}) controller and dash line refers reactive power drawn by the wind generator (WF_1) .)

VI. CONCLUSIONS AND FUTURE WORK

We have investigated the impact of wind farm dynamics on the available transfer capability of a heavily stressed transmission line. As the penetration level of fixed-speed conventional wind turbines increases the ATC substantially decreases. The amount of both static and dynamic compensations required for different levels of wind power integration has been reported in order to obtain the same ATC as conventional generators. A controller is designed to recover the original ATC. The designed controller is shown to be robust in the presence of interconnection effects and uncertainty. The performance of the proposed STATCOM controller is compared with a conventional PI-based STATCOM controller. The dynamic voltage stability as well as transient stability is improved and thereby the ATC increases significantly when the designed robust STATCOM controller is applied instead of a conventional PI-based STATCOM controller.

The proposed decentralized robust control has been limited to the considerations of nonlinear systems where only weak interconnections arise. For strong interconnections, the

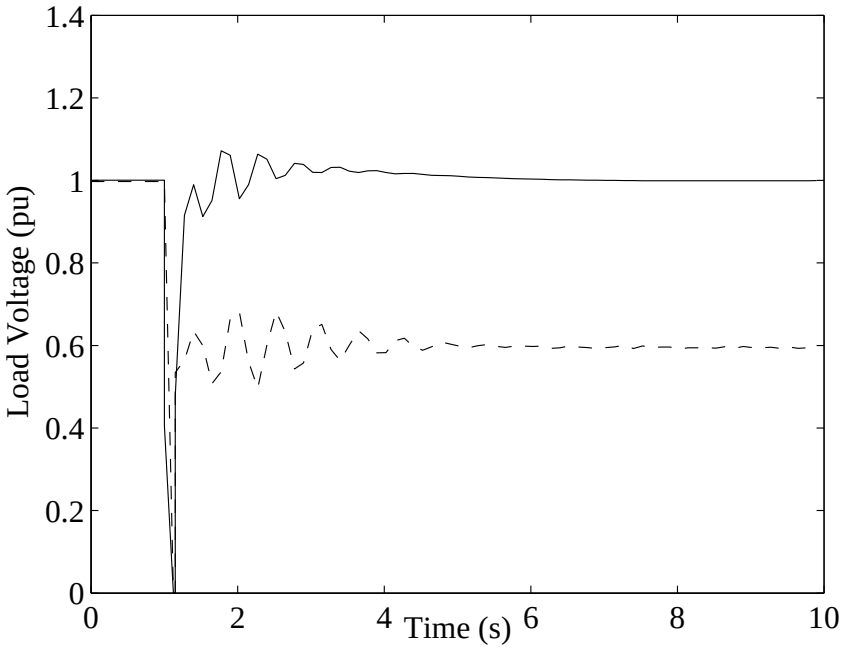

FIG. 11. Load voltage at bus 11 for a three phase fault on middle of one of the lines 6–7. (The solid line represents designed STATCOM control response, and dash line PI-based STATCOM.)

above analysis may be overconservative in terms of providing a quantitative measure of the input threshold. Future research will extend this work to strong interconnections and overlapping subsystems.

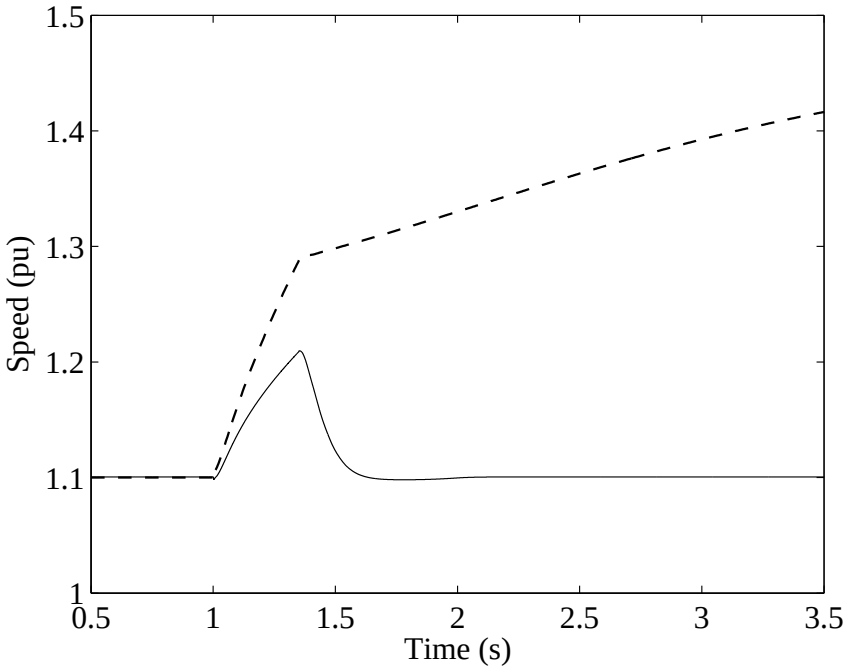

FIG. 12. Speed of wind generator (WF_1) for a three phase fault on middle of one of the lines 6–7. (The solid line represents designed STATCOM control response, and dash line PI-based STATCOM.)

APPENDIX - TEST SYSTEM DATA

Transmission lines- pu on 100 MVA base

Line	R	X	B
$5-6$	0.0000	0.0040	0.0000
$6-7$	0.0015	0.0288	1.173
$9-10$	0.0010	0.0030	0.0000

Transformers- pu on 100 MVA base

Line	R	X	*Ratio*
T_1	0.0000	0.0020	0.8857
T_2	0.0015	0.0045	0.8857
T_3	0.0010	0.0125	0.9024
T_4	0.0010	0.0030	1.0664
T_5	0.0010	0.0026	1.0800
T_6	0.0010	0.0010	0.9750
T_7	0.0010	0.0030	1.0000
T_8	0.0010	0.0030	1.0000

Machine parameters- machine 2 pu on 2200 MVA base and machine 3 on 1400 MVA

R_a	X_d	X_q	R_a	X_l	X'_d	X''_d	X''_q	T'_{d0}	T'_{q0}	T''_{d0}	T''_{q0}
0.0046	2.07	1.99	0.155	0.28	0.49	0.215	0.215	4.10	0.56	0.033	0.062

Induction generator parameters

Asynchronous Machines	
Power: 2 MW	$R_s = 0.0121$ pu
Voltage: 690 V	$X_s = 0.0742$ pu
Frequency, $f = 50$ Hz	$X_m = 2.7626$ pu
Self Damping, 0.008 pu	$R_r = 0.008$ pu
Rated Slip: 0.02	$X_r = 0.1761$ pu
Two Mass Model	STATCOM
$H_m = 2.6$s, $H_G = 0.22$s	Capacity: 12.5 MVA
$D_m = 3$ pu, $K_s = 141$ pu	$R_C = 0.01$ pu
Gearbox ratio: 23.75	$C = 300$ μF

REFERENCES

[1]T. Ackermann and L. Soder, Renewable and Sustainable Energy Reviews, Elsevier **6**, 67 (2002).

[2]North American Electric Reliability Council (NERC) (June, 2000).

[3]C. A. Ayasum and R. Fischl, in *Proc. NAPS* (Wyoming, 1997), pp. 464–469.

[4]R. P. Klump and T. J. Overbye, in *Proc. NAPS* (MIT, 1996), pp. 351–357.

[5]M. H. Gravener and C. Nwankpa, IEEE Trans. on Power Systems **14**, 512 (1999).

[6]M. Ramezani and M. R. Haghifam, in *IEEE Power and Energy Society General Meeting* (2007), pp. 1–6.

[7]C. A. Canizares, A. Berizzi, and P. Marannino, in *Proc. of Bulk Power System Dynamics and Control IV - Restructuring* (Santorini, Greece, 1998), pp. 633–641.

[8]Y. Xiao, Y. H. Song, C.-C. Liu, and Y. Z. Sun, IEEE Trans. on Power Systems **18**, 305 (2003).

[9]H. Farahmand, M. Roshidi-Nejad, and M. Fotirhi-Firoozabad, in *Proc. of Large Engineering systems Conference on Power Engineering* (2004), pp. 30–35.

[10]X. Yu, C. Singh, S. Jakovljevic, D. Ristanovic, and G. Huang, in *Transmission and Distribution Conference and Exposition* (2003), vol. 1, pp. 73–78.

[11]S. M. Sadeghzadeh, M. Ehsan, N. H. Said, and R. Feuillet, IEEE Trans. on Power Systems **13**, 917 (1998).

[12]L. Li, V. A. Ugrinovskii, and R. Orsi, Automatica **43**, 1932 (2007).

[13]E. D. Tuglie, S. M. Iannone, and F. Torelli, Electric Power Systems Research, Elsevier **78**, 382 (2008).

[14]I. R. Petersen, V. A. Ugrinovskii, and A. V. Savkin, *Robust Control Design Using H_∞ Methods* (Springer, London, 2000).

[15]P. Rao, M. L. Crow, and Z. Yang, IEEE Trans. on Power Delivery **15**, 131 (2000).

[16]T. Ackermann, *Wind Power in Power Systems* (John Wiley and Sons, Ltd, England, 2005).

[17]A. Feijo, J. Cidrs, and C. Carrillo, Electric Power Systems Research **56**, 121 (2000).

[18]K. Nandigam and B. H. Chowdhury, in *IEEE Power and Energy Society General Meeting* (2004), vol. 2, pp. 2012–2016.

[19]J. G. Slootweg, S. W. H. de Haan, H. Polinder, and W. L. Kling, IEEE Trans. on Power

Systems **18**, 144 (2003).

[20]B. Pal and B. Chaudhuri, *Robust Control in Power Systems* (Springer, USA, 2005).

[21]P. Kundur, *Power System Stability and Control* (Mcgraw-Hill, New York, 1994).

[22]IEEE Task Force, IEEE Trans. on Power Systems **8**, 472 (1993).

[23]G. Hamoud, IEEE Trans. on Power Systems **15**, 27 (2000).

[24]A. Kumar and S. C. Srivastava, IEEE Power Engineering Review **22**, 42 (2002).

[25]X. Luo, A. D. Patton, and C. Singh, IEEE Trans. on Power Systems **15**, 903 (2000).

[26]Y. Cheng, T. S. Chung, C. Y. Chung, and C. W. Yu, Electrical Power and Energy Systems, Elsevier **28**, 408 (2006).

[27]G. X. Athanasius, H. R. Pota, P. B. Subramanyam, and V. Ugrinovskii, in *46th IEEE Conference on Decision and Control* (New Orleans, Louisiana, USA, 2007), pp. 2427–2432.

[28]L. M. Fernandez, C. A. Garcia, J. R. Saenz, and F. Jurado, Energy Conversion and Management, Elsevier **50**, 691 (2009).

[29]A. J. Germond and R. Podmore, IEEE Trans. on Power Apparatus and Systems **PAS-97**, 1060 (1978).

[30]M. G. Yoon, V. A. Ugrinovskii, and M. Pszczel, IEEE Trans. on Automatic Control **52**, 311 (2007).

[31]J. Kueck, B. Kirby, T. Rizy, F. Li, and N. Fall, the Electricity Journal **19**, 27 (2006).